Large-Scale Dispersion of Clusters of Particles in the Atmosphere

S.-K. KAO AND A. A. AL-GAIN

University of Utah, Salt Lake City

(Manuscript received 5 June 1967, in revised form 5 December 1967)

ABSTRACT

The characteristics of the relative particle displacement tensor, the correlation functions, and spectra of the relative particle velocities at 200-, 500- and 850-mb levels are investigated. It is found that similarity and stability exist for the autocorrelation functions as well as the power spectra at various levels, which indicate that a quasi-stationary process exists in the large-scale relative diffusion in the atmosphere. The high frequency portion of the power spectra of both the zonal and meridional components of the relative velocities is found to be more or less proportional to k^{-3}; the relative meridional velocity shows a maximum at the low frequency end. The low frequency portion of the cross spectra of the zonal and meridional relative velocities at 850 mb shows an opposite transfer to that at 200 mb. The mean square of the relative zonal displacement at a level is found to be about twice that of the relative meridional displacement at that level. It is also found that anisotropy exists in the field of the large-scale turbulent dispersion and that the major axis of the dispersion is generally oriented in the ESE to WNW direction.

1. Introduction

Study of the characteristics of relative particle displacement is fundamental to the understanding of particle dispersion in instantaneous sources. Relative diffusion was investigated as early as 1923 by Roberts (1923) and later by many investigators (Richardson, 1926; Sutton, 1932; Batchelor, 1952; Frenkiel and Katz, 1956; Kellogg, 1956; Gifford, 1957; Machta *et al.*, 1957; Lin, 1960; Smith and Hay, 1961; Corrsin, 1962; Kao, 1962; Mesinger, 1965). These studies were primarily concerned with the rate of particle separation in relation to the particle distance. The main purpose of this paper is to investigate the characteristics of the relative velocity correlation functions, the power and cross spectra, as well as the relative particle displacement tensor at 200-, 500- and 850-mb levels in the atmosphere.

The accuracy in the prediction of turbulent diffusion depends on the degree of the statistical stationarity of the turbulent field of the motion. It is known that relative particle displacement would generally be affected by the nonstationary field of the motion. However, it is of practical importance that quasi-stationary processes would exist within various scales of the turbulence. One purpose of this paper is to test whether such a quasi-stationary process exists in the large-scale turbulent diffusion in the troposphere.

2. Theoretical consideration

In a recent paper (Kao, 1968) a theoretical analysis of diffusion of clusters of particles has been made. The following is a review of that part of Kao's paper applicable to this study.

We consider two particles simultaneously released in a field of turbulent motion which is statistically homogeneous but not isotropic. They will meander together with the main flow, but will also drift apart due to turbulent motion. We then consider the statistical average over an ensemble of such pairs. Let the ith component of their relative distance at time t be $x_{ri}(t)$, and that of their relative rate of separation be $v_{ri}(t)=dx_{ri}/dt$. We attempt to describe the statistical behavior of an ensemble of pairs of particles in terms of $\overline{x_{ri}(t)x_{rj}(t)}$ and $\overline{v_{ri}(t)v_{rj}(t)}$. To this end, we define the correlation function of the relative separation velocity as

$$R_{v_{ri}v_{rj}}(\tau)=\frac{\overline{v_{ri}(t)v_{rj}(t+\tau)}}{(\overline{v_{ri}^2v_{rj}^2})^{\frac{1}{2}}}. \tag{1}$$

We assume that the diffusion process is statistically stationary and random; thus,

$$R_{v_{ri}v_{rj}}(\tau)=R_{v_{rj}v_{ri}}(-\tau). \tag{2}$$

It can easily be shown by extending the analysis of absolute displacement of particles (Taylor, 1922) to relative particle displacement that

$$\overline{x_{ri}(t)y_{rj}(t)}=(\overline{v_{ri}^2v_{rj}^2})^{\frac{1}{2}}\int_0^t R_{v_{ri}v_{rj}}(\tau)d\tau+\overline{x_{ri}(t)y_{rj}(t)}. \tag{3}$$

By adding such equations with interchanged indices, we have

$$\frac{d}{dt}[\overline{x_{ri}(t)x_{rj}(t)}]=(\overline{v_{ri}^2v_{rj}^2})^{\frac{1}{2}}\times\int_0^t[R_{v_{ri}v_{rj}}(\tau)+R_{v_{rj}v_{ri}}(\tau)]d\tau. \tag{4}$$

Integration with respect to time gives

$$\overline{x_{ri}(t)x_{rj}(t)}=(\overline{v_{ri}^2v_{rj}^2})^{\frac{1}{2}}\int_0^t\int_0^\eta[R_{v_{ri}v_{rj}}(\tau)+R_{v_{rj}v_{ri}}(\tau)]d\tau d\eta+\overline{x_{ri}(0)y_{rj}(0)}. \quad (5)$$

The above equation can be shown to be expressed as

$$\overline{x_{ri}(t)x_{rj}(t)}=(\overline{v_{ri}^2v_{rj}^2})^{\frac{1}{2}}\int_0^t(t-\tau)[R_{v_{ri}v_{rj}}(\tau)+R_{v_{rj}v_{ri}}(\tau)]d\tau+\overline{x_{ri}(0)y_{rj}(0)}. \quad (6)$$

Since $R_{v_{ri}v_{rj}}(\tau)\approx R_{v_{ri}v_{rj}}(0)$ for small diffusion times, we have

$$\overline{x_{ri}(t)x_{rj}(t)}\approx(\overline{v_{ri}^2v_{rj}^2})^{\frac{1}{2}}R_{v_{ri}v_{rj}}(0)t^2+\overline{x_{ri}(0)y_{rj}(0)}. \quad (7)$$

For large diffusion times, we assume that $R_{v_{ri}v_{rj}}(\tau)\approx 0$, for $\tau>t^*$. Thus,

$$\overline{x_{ri}(t)x_{rj}(t)}\approx(\overline{v_{ri}^2v_{rj}^2})^{\frac{1}{2}}t\int_0^{t^*}[R_{v_{ri}v_{rj}}(\tau)+R_{v_{rj}v_{ri}}(\tau)]d\tau+\overline{x_{ri}(0)y_{rj}(0)}=2(\overline{v_{ri}^2v_{rj}^2})^{\frac{1}{2}}T_{rij}t+\overline{x_{ri}(0)y_{rj}(0)}, \quad (8)$$

where

$$T_{rij}=\frac{1}{2}\int_0^\infty[R_{v_{ri}v_{rj}}(\tau)+R_{v_{rj}v_{ri}}(\tau)]d\tau$$

is a Lagrangian relative time scale.

It can be shown that the cross spectrum of the relative velocity takes the form

$$E_{v_{ri}v_{rj}}(n)=2(\overline{v_{ri}^2v_{rj}^2})^{\frac{1}{2}}\int_0^\infty[R_{v_{ri}v_{rj}}(\tau)+R_{v_{rj}v_{ri}}(\tau)]\times\cos 2\pi n\tau d\tau. \quad (9)$$

For convenience of comparison of spectra at various levels and seasons, we use the normalized spectra

$$F_{v_{ri}v_{rj}}(n)=\frac{E_{v_{ri}v_{rj}}(n)}{(\overline{v_{ri}^2v_{rj}^2})^{\frac{1}{2}}},$$

where n is the frequency. The inverse transform of Eq. (9) gives

$$R_{v_{ri}v_{rj}}(\tau)+R_{v_{rj}v_{ri}}(\tau)=\frac{2}{(\overline{v_{ri}^2v_{rj}^2})^{\frac{1}{2}}}\times\int_0^\infty E_{v_{ri}v_{rj}}(n)\cos 2\pi n\tau dn. \quad (10)$$

Substituting (10) into (6), and integrating with respect to τ, we obtain

$$\overline{x_{ri}(t)x_{rj}(t)}=t^2\int_0^\infty E_{v_{ri}v_{rj}}(n)\left(\frac{\sin\pi nt}{\pi nt}\right)^2dn+\overline{x_{ri}(0)x_{rj}(0)}. \quad (11)$$

For small diffusion times, Eq. (11) may be approximated by

$$\overline{x_{ri}(t)x_{rj}(t)}\approx t^2\int_0^\infty E_{v_{ri}v_{rj}}(n)dn+\overline{x_{ri}(0)x_{rj}(0)}. \quad (12)$$

Thus, at the initial stage of diffusion the separation of particles is affected by turbulent motion of all scales.

For large diffusion times, Eq. (11) may be approximated by

$$\overline{x_{ri}(t)x_{rj}(t)}\approx\tfrac{1}{2}E_{v_{ri}v_{rj}}(0)t+\overline{x_{ri}(0)x_{rj}(0)}. \quad (13)$$

Thus, for large diffusion times the separation of particles is primarily affected by the turbulent motion of large scale.

We define a time dependent turbulence diffusivity

$$\epsilon_{rij}(t)=\frac{1}{2}\frac{d}{dt}[\overline{x_{ri}(t)x_{rj}(t)}]. \quad (14)$$

For small diffusion times, substitution of (12) and (7) into (14) gives

$$\epsilon_{rij}(t)=t\int_0^\infty E_{v_{ri}v_{rj}}(n)dn=(\overline{v_{ri}^2v_{rj}^2})^{\frac{1}{2}}t. \quad (15)$$

For large diffusion times, substitution of (8) and (13) into (14) gives

$$\epsilon_{rij}(t)=\tfrac{1}{4}E_{v_{ri}v_{rj}}(0)=(\overline{v_{ri}^2v_{rj}^2})^{\frac{1}{2}}T_{rij},$$

i.e., a constant.

In this study, we consider diffusion in horizontal planes only. Let x and y axes of a Cartesian coordinate system be directed toward the east and north, respectively. Therefore, $\overline{x_r^2}(t)$ and $\overline{y_r^2}(t)$ give the measures of the x and y components of the relative separation of particles at time t; $\overline{x_r(t)y_r(t)}$ represents the correlation of the particles separation along the x and y components of the axis, which together with $\overline{x_r^2}(t)$ and $\overline{y_r^2}(t)$ determine the orientation of the principal axes of diffusion.

Let (x',y') be a new Cartesian coordinate system whose axes coincide with the principal axes of diffusion. Therefore,

$$\overline{x_r'(t)y_r'(t)}=0. \quad (16)$$

Let α be the angle between x and x' axis, measured in the counterclockwise direction. We have

$$x_r'=x_r\cos\alpha+y,\ \sin\alpha,$$
$$y_r'=-x_r\sin\alpha+y_r\cos\alpha.$$

By use of (16) we obtain

$$[-\overline{x_r^2}(t)+\overline{y_r^2}(t)]\sin\alpha\cos\alpha+\overline{x_ry_r}(\cos^2\alpha-\sin^2\alpha)=0.$$

Thus,

$$\alpha(t)=\tfrac{1}{2}\tan^{-1}\left(\frac{2\overline{x_r(t)y_r(t)}}{\overline{x_r^2}(t)-\overline{y_r^2}(t)}\right), \tag{17}$$

and

$$\left.\begin{aligned}\overline{x_r'^2}(t)&=\overline{x_r^2}(t)+\overline{x_r(t)y_r(t)}\tan\alpha(t)\\ \overline{y_r'^2}(t)&=\overline{y_r^2}(t)-\overline{x_r(t)y_r(t)}\tan\alpha(t)\end{aligned}\right\}. \tag{18}$$

Since ϵ_{rij} is a tensor of second order, its relation to the turbulence diffusivity $\epsilon_{ri''j''}(t)$ in a Cartesian coordinate system (x'',y'') is therefore

$$\epsilon_{rj''k''}=\epsilon_{rij}c_{ij''}c_{jk''},$$

where $c_{ij''}$ and $c_{jk''}$ are the direction cosines between the i and j'' axes and between the j and k'' axes, respectively. Let (x'',y'') be so oriented such that $\epsilon_{rx''y''}=0$, and let α_ϵ be the angle between the x and x'' axes. It can then be shown that

$$\alpha_\epsilon(t)=\tfrac{1}{2}\tan^{-1}\left[\frac{\epsilon_{rxy}(t)}{\epsilon_{rxx}(t)-\epsilon_{ryy}(t)}\right], \tag{19}$$

and

$$\epsilon_{rx''x''}=\epsilon_{rxx}+\epsilon_{rxy}\tan\alpha_\epsilon,$$
$$\epsilon_{ry''y''}=\epsilon_{ryy}-\epsilon_{rxy}\tan\alpha_\epsilon.$$

Therefore,

$$\alpha_\epsilon=\tfrac{1}{2}\tan^{-1}\left\{\tan2\alpha+\frac{(\overline{x_r^2}-\overline{y_r^2})}{\dfrac{d}{dt}(\overline{x_r^2}-\overline{y_r^2})}\frac{d}{dt}(\tan2\alpha)\right\}.$$

It can be seen that

$$\alpha_\epsilon=\alpha \quad \text{when} \quad \frac{d\alpha}{dt}=0.$$

In this analysis we consider that each cluster consists of N particles; their relative displacement tensor may thus be computed as

$$\overline{x_{ri}(t)x_{rj}(t)}=\frac{2}{N(N-1)}\times\sum_{n=m+1}^{N}\sum_{m=1}^{N-1}(x_{i,m}-x_{i,n})(x_{j,m}-x_{j,n}), \tag{20}$$

for $i,j=1,2$.

In this study 972 trajectories have been computed (9 trajectories in each run) and a total of 3888 particle pairs have been analyzed.

3. Source of data and analysis

One purpose of this study was to analyze the two-dimensional large-scale continuous dispersion based on a statistically stationary analysis of stream function trajectories and velocities, and to present information concerning the relative diffusion of a cluster of particles. Stream functions for the 200-, 500- and 850-mb levels were extracted from National Meteorological Center (NMC) tapes and analyzed for the entire year of 1964. Nine particles formed into a circular cluster having a diameter of 175 km centered at 46.7N and 141.4W was released at the aforementioned levels. This initial position was chosen mainly because a considerable portion of the resulting trajectories would be over the United States, where upper-air data are abundant and more accurate. Furthermore, trajectories of particles released at this latitude can be traced up to eight days without going off 18N, the lower limit of the NMC map.

Stream function maps were available at 0000 and 1200 GMT for every day of 1964 except for a few missing cases. Each cluster of nine particles was initiated at 1200 GMT and their trajectories were obtained for 8 days, or 192 hr. Thus, 17 consecutive maps were necessary for each run. Three clusters were released each month. Although an attempt was made to achieve ideal spacing by releasing the three clusters, say, on the 1st, 11th and the 21st of each month, respectively, the fact that some maps would be missing during the month necessitated a considerable deviation from those dates. Another attempt was made to achieve the same release dates for all three levels. This objective has been achieved in most cases. However, on a few occasions the missing maps did not coincide at all three levels, and sometimes a particle trajectory, say on the 850-mb level, leaves the map area (travels south of 20N), in which case the whole run is rejected and a nearby date chosen for re-release.

The trajectories were constructed over 2-hr time steps. The velocity used to locate each new point on a trajectory was arrived at by averaging two velocities. For example, to compute the second position of a trajectory, the velocity at the initial position was computed from stream functions at the initial time. Then a preliminary position was calculated by assuming a constant velocity for the particle for the 2-hr period. A second velocity was computed from the stream function field in effect at the preliminary position at the end of the time step. Then the vector average of the two velocities was taken as the mean velocity of the particle throughout the 2-hr period, and the second position calculated accordingly. Ninety-six such cycles were required for constructing each particle trajectory. To obtain velocities at times between the available maps, intermediate maps had to be constructed. By interpolation they were constructed for times 2, 4, 6, 8 and 10 hr after each map on the tape. A program was designed by which the 7044 IBM computer read the tape, constructed the intermediate maps and then constructed the trajectories.

4. The autocorrelation functions and power spectra

For each season at each of the 200-, 500- and 850-mb levels, we have computed the Lagrangian autocorrelation and cross-correlation functions for the relative

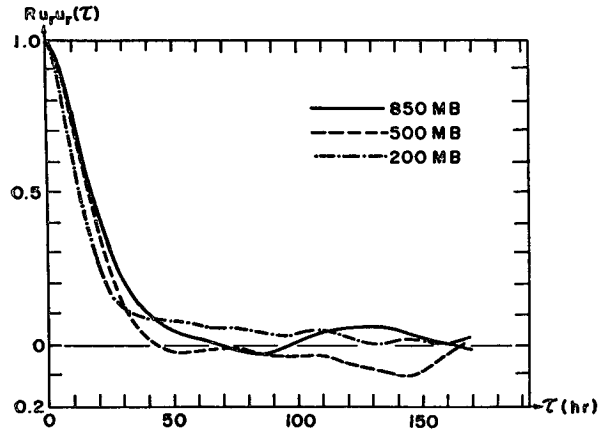

FIG. 1. Autocorrelation functions of the zonal component of the relative velocity at 200, 500 and 850 mb.

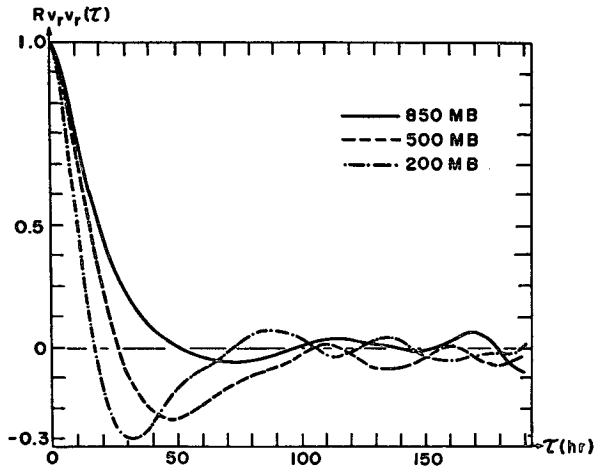

FIG. 2. Autocorrelation functions of the meridional component of the relative velocity.

velocities. With the use of these correlation functions, the power spectra are computed. To examine the characteristics and similarities in the autocorrelation functions, the yearly autocorrelation for the zonal and meridional components of the relative velocities are shown in Figs. 1 and 2, where, in both diagrams, the solid lines represent the autocorrelation distribution at the 850-mb, the dashed lines at the 500-mb, and the dashed-dot lines at the 200-mb level.

The autocorrelation for all levels for the zonal components of the relative velocity shows the characteristic of an exponential distribution, whereas those for the meridional component of the velocities show the combination of an exponential function and a cosine function with a damping amplitude. They agree well with the theoretical expressions deduced from a planetary wave model derived by Kao (Kao, 1962). Inspecting the aforementioned diagrams further, it can be seen that the minimum correlation for the meridional component of the velocity is attained at a smaller time lag for the higher levels. That is, at the 200-mb level the minimum correlation is attained in about 40 hr, whereas at the 500- and 850-mb levels the minimum correlation is attained at 50 and 70 hr, respectively. Similarly, the decrease in the correlation for the zonal component is greater for the higher levels. This indicates that dispersion of particles in the lower levels is affected more by eddies of low frequencies than those on the higher levels. The seasonal and annual power spectra were computed. The annual zonal and meridional component of the power spectra are presented in Figs. 3 and 4. The stability of the autocorrelation functions and similarity in the power spectra of the relative velocities at various levels indicate that a quasi-stationary process exists in the large-scale turbulence in the atmosphere.

The monotonic decreasing behavior of the autocorrelation function of the relative zonal velocity at the 200-, 500- and 850-mb levels indicates that the greatest energy is at the lowest frequencies. As was pointed out in the preceding paragraph, the minimum of the correlation function of the meridional components of the relative velocity occurs at a smaller value for the higher levels (Fig. 2); thus, the energy peak of the

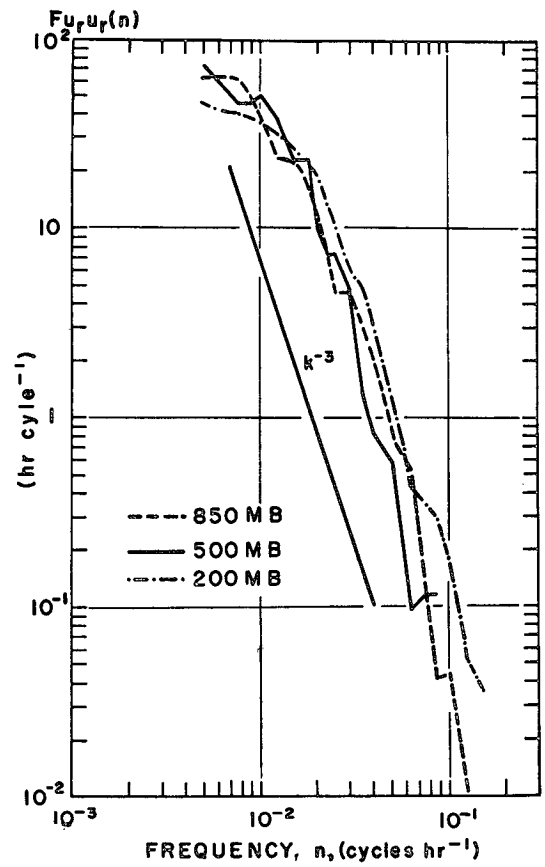

FIG. 3. Normalized power spectra of the zonal component of the relative velocity.

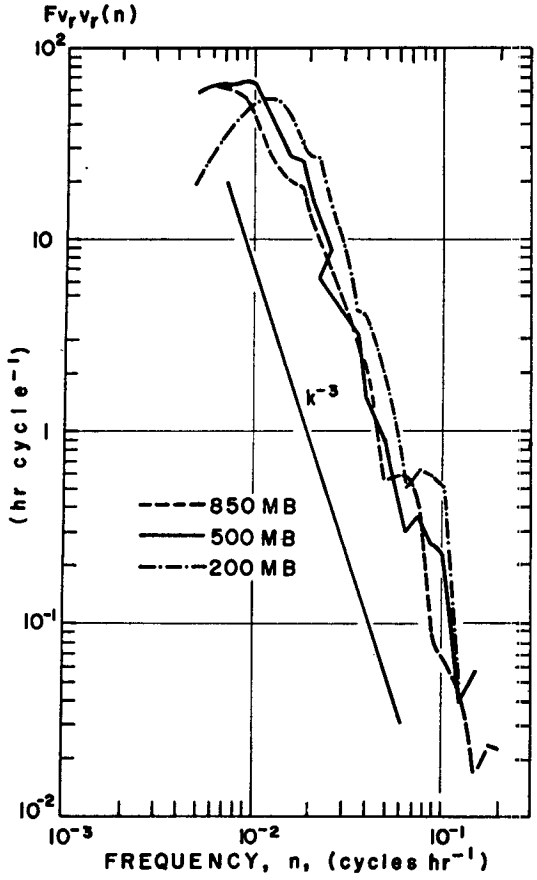

FIG. 4. Normalized power spectra of the meridional component of the relative velocity.

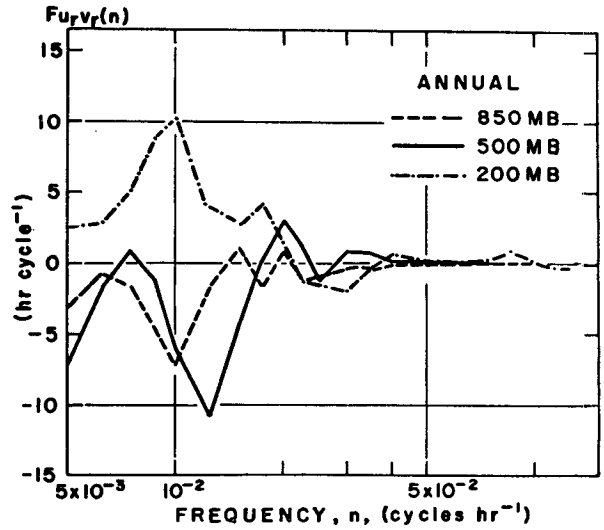

FIG. 6. Cross spectra of the zonal and meridional components of the relative velocity.

meridional component of the velocity occurs at a lower frequency for the lower levels as shown in Fig. 4. In these figures, the lower limit of the frequency is estimated by $(2T_{max})^{-1}$, which for maximum interval between observation $T_{max}=8$ days, is about 0.003 cycle hr^{-1}, and the upper limit of the frequency is estimated by $\bar{v}_r/\bar{d}$, which for mean relative velocity $\bar{v}_r=10$ m sec^{-1} and mean grid distance $\bar{d}=350$ km, is about 0.103 cycle hr^{-1}.

Figs. 3 and 4 show that the turbulent kinetic energy generally decreases with increasing frequency, which indicates that the rate of relative dispersion of particles generally increases with the size of particle cluster. In these figures, a line for k^{-3} is shown for comparison purpose with the spectral distribution at the high frequency range of the spectra.

It may be noted from the distribution of the Lagrangian autocorrelation functions and power spectra of the relative velocity at 200 mb and those of a single particle at 300 mb (Kao, 1965) that the minimum of the relative meridional Lagrangian velocity occurs somewhat later than that of the single particle, and

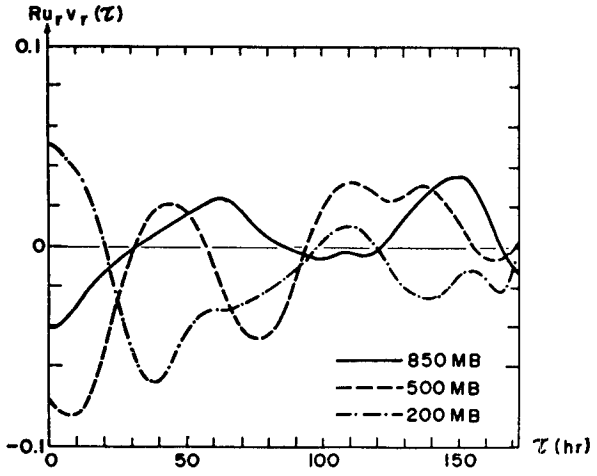

FIG. 5. Cross-correlation functions of the zonal and meridional components of the relative velocity.

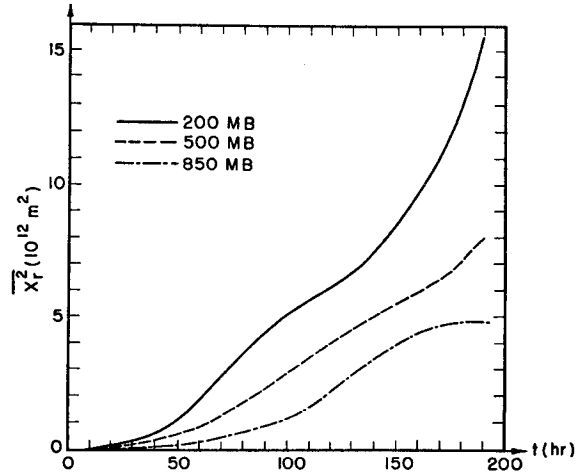

FIG. 7. Mean squares of the zonal components of the relative particle displacement.

TABLE 1. Mean variances and covariances of relative velocities (m^2 sec^{-2}).

	200 mb			500 mb			850 mb		
Season	$\overline{u_r'^2}$	$\overline{v_r'^2}$	$\overline{u_r'v_r'}$	$\overline{u_r'^2}$	$\overline{v_r'^2}$	$\overline{u_r'v_r'}$	$\overline{u_r'^2}$	$\overline{v_r'^2}$	$\overline{u_r'v_r'}$
Winter	247.99	179.97	12.36	126.82	129.50	−16.33	69.46	50.79	−4.50
Spring	248.31	185.14	21.06				25.74	22.28	0.16
Summer	142.90	154.18	10.03	77.53	70.53	0.78	9.92	12.44	−0.86
Autumn	179.08	211.98	−3.23				34.69	29.15	0.18
Annual	204.57	182.82	10.05	102.17	100.01	−7.78	34.95	28.67	−1.26

The covariances of the relative velocities have a negative annual value at the 500- and 850-mb levels, but a positive value at the 200-mb level.

that the slope of the power spectra of the former is slightly steeper than that of the latter. However, the characteristic energy peak of the power spectra of the meridional velocity remains.

5. The cross-correlation functions and cross spectra

To examine the characteristics of the anisotropy of the field of relative turbulence and diffusion, the cross correlation of the zonal and meridional components of the velocity was computed for seasonal as well as annual averages, for four seasons at the 200- and 850-mb levels, and winter and summer at the 500-mb level. The annual cross-correlation functions are shown in Fig. 5. The annual normalized cross spectra given in Fig. 6 show that the minima for the lower levels (500, 850 mb) occur at more or less the same frequency at which the upper level has its maximum. This indicates that the contribution of the anisotropy in the relative turbulent motion to the diagonal components of the relative displacement tensor [Eq. (11)] in the upper level has an opposite sign to that in the lower levels. In general, for small diffusion times, the degree of anisotropy of turbulent diffusion is affected by the cross spectra of all frequencies, but primarily by that of the low frequency components for large diffusion times. Further discussion of the degree of anisotropy in turbulent diffusion will be given in later sections.

To obtain the power and cross spectra, the normalized power and cross spectra should be multiplied by the corresponding variances of the relative velocity. The mean variances of the relative velocity for various seasons shown in Table 1 indicate that their values generally increase with height and have minima occurring in the summer. However, at 850 mb their maxima occur in the winter, whereas at 200 mb the maximum variance of the relative zonal velocity occurs in the spring, and that of the meridional component occurs in the autumn.

6. The relative displacement of particles as a function of time

As a measure of the relative zonal and meridional particle separations as functions of time, the mean squares of these separations are computed at 2-hr intervals from the 36 runs, nine for each of the four seasons at the 200- and 850-mb levels, and for the winter and summer seasons at the 500-mb level. They are shown in Figs. 7–9. For all experiments, the initial mean distance of the particle separation were $4.11\times1^{11}0$ m^2 for $\overline{x_r^2}$ and $\overline{y_r^2}$ at all levels.

Fig. 7 shows the mean square relative zonal displacements for 200, 500 and 850 mb. It is seen from this figure that the zonal relative particle displacements monotonically increase with time at all levels, and that the relative displacement at 200 mb is generally greater than that at 500 mb, whereas the latter is greater than that at 850 mb. The relative zonal displacement at 200 mb is about twice that at 850 mb.

The mean square meridional relative displacements for the 200-, 500- and 850-mb levels are shown in Fig. 8. Again, the meridional relative displacements increase

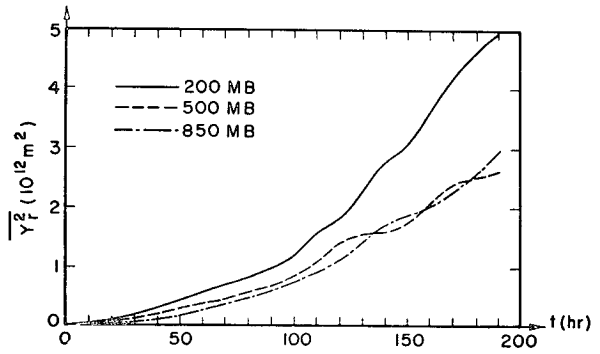

FIG. 8. Mean squares of the meridional component of the relative particle displacement.

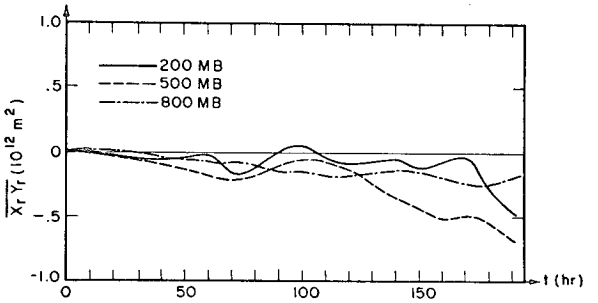

FIG. 9. Mean correlations of the zonal and meridional components of the relative particle displacement.

TABLE 2. Angle (degrees) between principal axis of diffusion and x axis.

Level (mb)	Time (hours) 10	20	30	40	50	60	70	80	90	100	110	120	130	140	150	160	170	180	190
200	−81	−71	−48	−25	−15	−14	−18	−18	−15	−12	−10	−6	−5	−6	−8	−7	−6	−7	−7
500	−51	−38	−26	−20	−19	−20	−14	−9	−5	−3	−2	−4	−6	−6	−7	−8	−8	−7	−7
850	64	90	−74	−66	−59	−46	−33	−31	−42	−43	−49	−59	−66	−59	−38	−21	−6	5	10

monotonically with time. The relative displacement at 200 mb is generally greater than that at the 500- and 850-mb levels. One distinct feature which appeared in the relative meridional displacements is the wavy type of oscillation, which may be the result of the influence of the planetary waves in the atmosphere.

A simple plot of the mean square relative zonal and meridional displacements vs time in a logarithmic scale indicates that the mean square relative zonal and meridional particle separations at all levels are more or less proportional to t^2, except for the mean square relative zonal displacement at 850 mb which is more or less proportional to t^3. It may be noted that the mean squares of the relative zonal and meridional separations of particles must eventually reach their respective limiting values since both the zonal and meridional dimensions of the atmosphere are finite.

The diagonal components of the relative displacement tensor are computed for the 200-, 500- and 850-mb levels, and are shown in Fig. 9. They are mostly negative at all levels, which indicates that the major axis of the large-scale particle dispersion is mostly oriented in an ESE to WNW direction. The angles between the major axis of dispersion and the x axis for various seasons and at the three levels are computed with the use of Eq. (17) and are listed in Table 2. In general, the angle α becomes steady at large diffusion times and its magnitude at 500 mb is smaller than at the other two levels.

Fig. 10 shows the mean displacement of the center of mass of the clusters of particles at the 200-, 500- and 850-mb levels. Particles at the 200- and 500-mb levels generally move zonally, whereas those at the 850-mb level tend to move toward the southeast.

TABLE 3. Percentage relationship between diffusion along the major and zonal axes (upper) and along the minor and meridional axes (lower).

	Time (hours) 20	40	60	80	100	120	140	160	180	190
200 mb										
Winter	55	28	3	0	1	9	26	5	4	2
Spring	1	7	10	3	1	0	1	1	1	1
Summer	7	0	0	4	4	4	12	11	3	1
Autumn	66	15	4	9	4	1	1	1	1	1
500 mb										
Winter	3	8	10	4	1	3	4	5	3	1
Summer	79	9	7	1	0	4	0	0	0	0
850 mb										
Winter	206	154	26	4	3	1	1	0	1	2
Spring	26	33	18	11	6	1	1	0	1	0
Summer	99	92	67	56	116	91	169	104	77	81
Autumn	268	250	55	11	17	32	21	3	0	1

	Time (hours) 20	40	60	80	100	120	140	160	180	190
200 mb										
Winter	−64	−45	−13	−1	−2	−8	−21	−5	−5	−2
Spring	−10	−17	−25	−14	−8	−2	−5	−7	−16	−15
Summer	−6	0	0	−19	−19	−15	−30	−26	−8	−3
Autumn	−42	−33	−22	−45	−16	−5	−6	−4	−3	−5
500 mb										
Winter	−5	−23	−30	−12	−3	−8	−11	−10	−7	−5
Summer	−50	−9	−12	−1	−1	0	0	0	0	−2
850 mb										
Winter	−67	−70	−22	−6	−4	−2	−1	0	−2	−2
Spring	−22	−46	−38	−36	−15	−1	−1	−1	−2	−1
Summer	−56	−60	−47	−39	−54	−41	−64	−51	−44	−46
Autumn	−73	−82	−54	−13	−17	−26	−18	04	0	−2

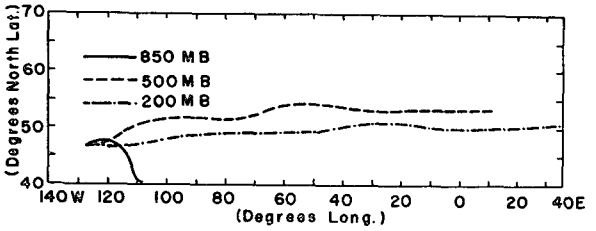

FIG. 10. Mean displacements of the center of mass of particles at 200, 500 and 850 mb.

Because of the increase in the zonal velocity with height, an initially vertical air column would generally be stretched toward the northwest and disperses both horizontally and vertically.

The percentage difference between diffusion along the major and zonal axes and between the minor and meridional axes have been computed with the use of (18), i.e.,

$$100\left(\frac{\overline{x_r'^2}(t)}{\overline{x_r^2}(t)}-1\right)=100\left(\frac{\overline{x_r(t)y_r(t)}}{\overline{x_r^2}(t)}\right)\tan\alpha(t),$$

$$100\left(\frac{\overline{y_r'^2}(t)}{\overline{y_r^2}(t)}-1\right)=100\left(\frac{\overline{x_r(t)y_r(t)}}{\overline{y_r^2}(t)}\right)\tan\alpha(t),$$

and are presented in Table 3. The percentage difference is a minimum at the 500-mb level and generally decreases with increasing diffusion times. Its magnitude at 850 mb is generally greater than at 200 mb.

Acknowledgments. The authors wish to thank David C. Powell and Larry L. Wendell for their help in programming some of the computation used in this study. This research has been partially supported by the Division of Biology and Medicine of the U. S. Atomic Energy Commission, under Contract AT(11-1)-1585.

REFERENCES

Batchelor, G. K., 1952: Diffusion in the field of homogeneous turbulence. 2, The relative motion of particles. *Proc. Cambridge Phil. Soc.*, **48**, 345–362.

Corrsin, S., 1962: Theories of turbulent diffusion. *Mecanique de la Turbulence*, Paris, Centre National de la Recherche Scientifique, 27–52.

Frenkiel, F. N., and I. Katz, 1956: Studies of small-scale turbulent diffusion in the atmosphere. *J. Meteor.*, **13**, 388–394.

Gifford, F., 1957: Relative atmospheric diffusion of smoke puffs. *J. Meteor.*, **14**, 410–414.

Kao, S.-K., 1962: Large-scale turbulent diffusion in a rotating fluid with applications to the atmosphere. *J. Geophys. Res.*, **67**, 2347–2359.

——, 1965: Some aspects of the large-scale turbulence and diffusion in the atmosphere. *Quart. J. Roy. Meteor. Soc.*, **91**, 10–17.

——, 1968: Relative dispersion of particles in a stratified, rotating atmosphere. *J. Atmos.*, **25** (in press).

Kellogg, W. W., 1956: Diffusion of smoke in the stratosphere. *J. Meteor.*, **13**, 241–250.

Lin, C. C., 1960: On a theory of dispersion by continuous movements. *Proc. Natl. Acad. Sci. U. S.*, **46**, 566–570, 1147–1153.

Machta, L., H. L. Hamilton, L. F. Hubert, R. J. List and K. M. Nagler, 1957: Airborne measurement of atomic debris. *J. Meteor.*, **14**, 165–175.

Mesinger, E., 1965: Behavior of a very large number of constant-volume trajectories. *J. Atmos. Sci.*, **22**, 479–492.

Richardson, L. F., 1926: Atmospheric diffusion shown on a distance-neighbor graph. *Proc. Roy. Soc. (London)*, **A110**, 709–737.

Roberts, O. F. T., 1923: The theoretical scattering of smoke in a turbulent atmosphere. *Proc. Roy. Soc. (London)*, **A104**, 640–654.

Smith, F. B., and J. S. Hay, 1961: The expansion of clusters of particles in the atmosphere. *Quart. J. Roy. Meteor. Soc.*, **87**, 82–101.

Sutton, O. G., 1932: A theory of eddy diffusion in the atmosphere. *Proc. Roy. Soc. (London)*, **A135**, 143–165.

Taylor, G. I., 1922: Diffusion by continuous movement. *Proc. London Math. Soc.*, **20**, 196–212.